Inertial Navigation System Aided by GPS and Selective Frequency Contents of Vector Measurements

J.F. Vasconcelos*, P. Oliveira†, Carlos Silvestre‡

Instituto Superior Técnico, Institute for Systems and Robotics, Lisbon, Portugal

This paper proposes an aiding technique to enhance error estimation in low-cost strapdown inertial navigation systems with application to Unmanned Air Vehicles (UAVs). The paper summarizes a high-accuracy, multi-rate integrated Global Positioning System/Inertial Navigation System (GPS/INS) using Extended Kalman Filter (EKF) for error compensation. A proposed new technique decomposes and optimally integrates the magnetic and gravitational observations in the EKF, taking into account the vehicle's dynamics bandwidth information to properly trace inertial motion. In particular, the paper evidences that inertial misalignment errors and biases can be effectively estimated resorting to the gravity vector low frequency information embodied in accelerometer measurements. The performance of the overall INS aiding architecture is assessed in simulation, and results obtained about UAV typical trajectories are presented and discussed.

Nomenclature

Notation

$\bar{\mathbf{s}}$	Nominal vector
$\mathbf{s}_r$	Sensor measurement of vector $\bar{\mathbf{s}}$
$\mathbf{s}$	Compensated vector
$\hat{\mathbf{s}}$	Estimated vector
$\delta\mathbf{s} = \mathbf{s} - \bar{\mathbf{s}}$	Vector error
$[\mathbf{s}\times]$	Cross product operator for vector $\mathbf{s}$
$\|\mathbf{s}\|$	Magnitude of vector $\mathbf{s}$
${}^F\mathbf{s}$	Vector expressed in coordinate frame $\{F\}$
$\mathbf{A}'$	Transpose of matrix $\mathbf{A}$

Nomenclature

$\{E\}, \{B\}$	Earth and body coordinate frames
${}^B\mathbf{a}_{SF}$	Specific force expressed in body frame
$\mathbf{a}, \mathbf{v}, \mathbf{p}$	Acceleration, velocity, and position expressed in Earth frame
$\boldsymbol{\omega}$	Body angular rate expressed in body frame
$\mathbf{b}_a, \mathbf{b}_\omega$	Accelerometer and rate gyro triads biases expressed in body frame
$\mathbf{g}$, $\mathbf{m}$	Earth gravitational and magnetic fields
$\mathbf{n}_a, \mathbf{n}_\omega, \mathbf{n}_m$	Accelerometer, rate gyro, and magnetometer triads zero mean white noises with variances $\sigma_a^2, \sigma_\omega^2, \sigma_m^2$
$\boldsymbol{\lambda}$	Rotation vector with magnitude $\lambda = \|\boldsymbol{\lambda}\|$
${}^E_B\mathbf{R}(\boldsymbol{\lambda})$	Rotation matrix from body to Earth coordinate frames, parameterized by $\boldsymbol{\lambda}$
$\mathcal{R}$	Shorthand notation for ${}^E_B\mathbf{R}(\boldsymbol{\lambda})$
$\mathbf{I}_{n\times n}$	N-dimensional identity matrix

*PhD Student, Department of Electrical Engineering and Computer Science (DEEC), and Institute for Systems and Robotics (ISR), Instituto Superior Técnico (IST), Av. Rovisco Pais, 1, Torre Norte, 8° Andar, 1049-001, Lisboa, Portugal, AIAA Student Member. E-mail: jfvasconcelos@isr.ist.utl.pt

†Assistant Professor, DEEC, ISR, IST. E-mail: pjcro@isr.ist.utl.pt

‡Assistant Professor, DEEC, ISR, IST, AIAA Member. E-mail: cjs@isr.ist.utl.pt

Subscripts and Superscripts

k	Time index
$-, +$	Predicted and updated filter states

I. Introduction

High maneuverability, versatility, and complex dynamics make model-scale helicopters a cost-effective Unmanned Air Vehicle (UAV) platform with wide and valuable operational capabilities to perform realistic missions. Among others, they include bridge monitoring, accurate terrain and natural resource surveying, and crop fields spraying. The use of these platforms in surveying and monitoring missions requires low-cost, ultra light weight, high performance, robust navigation systems, that can accurately estimate the UAV's position and attitude. These facts raised, in the last years, the Autonomous Vehicles scientific community awareness towards strapdown navigation systems.

Accuracy and performance specifications often foster higher requirements for such cost effective navigation systems. Low-cost aiding sensors require more complex filtering techniques in order to meet performance specifications and to tackle noise and bias effects. New onboard aiding compensation techniques and multiple inertial sensor error models have been recently taken into account in the navigation system's structure, to enhance its performance and robustness.

This paper proposes a solution to include vector observations and vehicle dynamics bandwidth information directly in the Extended Kalman Filter (EKF). Attitude measurements based on vector observations are usually integrated using standalone attitude estimation algorithms. In this work, the Kalman filter acts as an attitude determination algorithm using magnetometer and gravity observations as direct inputs. Rate gyro and accelerometer biases compensation enhancements are illustrated, using magnetometer measurements and selective frequency contents from gravity information, provided by the accelerometer triad readings. An arbitrary number of time-varying aiding vector readings and optimal sensor error modeling in the EKF are made possible by using the proposed architecture.

Past work on attitude aiding devices focused on a Magneto-Pendular Sensor (MPS), Ref. 1. This standalone unit computed an attitude estimate based on the Earth's gravitational and magnetic fields, which was externally fed to a Non-linear Complementary Kalman Filter. The new technique proposed in this paper decomposes and optimally integrates the magnetic and gravitational observations in the EKF, taking into account the vehicle's dynamics bandwidth information to properly trace inertial motion.

Classical GPS/INS involving inertial sensor biases estimation are found to hold only partial observability for a time-invariant configuration. As convincingly argued in Refs. 2–4, time-varying in-flight characteristic maneuvers and disturbances excite the remaining observable variables and turn the system to full observability under specific assumptions. Recent work has been directed towards replacing these on-flight alignment maneuvers by equipping the filter with additional information sources, namely aiding sensors or vehicle dynamic model information, see Refs. 4–6. Moreover, a valuable survey on attitude determination methods based on aiding vector observations is provided in Ref. 7, where a Matrix Kalman Filter is designed to determine attitude rotation matrix and a set of normalization procedures is proposed.

The Inertial Navigation System (INS) is the backbone algorithm that performs attitude, velocity and position numerical integration from rate gyro and accelerometer triads data, rigidly mounted on the vehicle structure (strapdown configuration). Global attitude high-precision INS algorithms that account for high frequency attitude, velocity and position motions (denoted as coning, sculling and scrolling respectively) are developed in Refs. 8–10. Interestingly enough, Ref. 11 proposes a technique to convert the high accuracy attitude algorithms into its velocity/position counterpart.

For highly maneuverable vehicles, the INS numerical integration must properly address the fast dynamics of inertial sensors output, to avoid estimation errors buildup. Usually INS algorithm execution rates are set as a trade-off between the available hardware and the performance requirements.[8–10] Simulation environments and trajectory profiles to tune the algorithm's repetition rate according to the accuracy requirements are thoroughly described by Savage[12] and some pencil-and-paper algorithm evaluation procedures are presented in Refs. 8, 9. In recent vehicle literature Refs. 4–6, 13, 14, the EKF is adopted to dynamically compensate for non-ideal sensor characteristics that otherwise would yield unbounded INS errors.

The proposed navigation system architecture is depicted in Figure 1. The system is based on a high-precision INS to compute attitude, velocity and position, and performs error correction using a direct-

feedback configuration. The EKF estimates the attitude error using an unconstrained, locally non-singular attitude parameterization that can be assumed locally linear, as discussed by Markley.[15] The attitude error parameterization is reset after being applied to compensate, in a non-linear fashion, the global attitude estimate, described in Direction Cosine Matrix (DCM) form. This incremental procedure can be regarded as a storage technique that prevents the filter's attitude error estimates to fall into singular configurations. In this work, the attitude error is parameterized using the rotation vector representation in Earth coordinates. Other equivalent frame coordinates and attitude parameterizations can be used, such as Gibbs vector and Modified Rodrigues Parameters,[15,16] that hold identical mathematical first order relationships.

The paper is organized as follows. Section II briefly discusses the INS algorithm adopted in this work. In Section III, EKF equations are developed to model inertial sensor errors, and error correction procedures are detailed. The main contribution of this paper is derived and illustrated in Section IV where generalized vector readings are optimally introduced into the EKF. The technique is illustrated for GPS, magnetometer measurements, and gravity vector information obtained from selective frequency contents of accelerometer readings. It is also pointed out how vehicle dynamics bandwidth information can be merged into the EKF, to enhance the overall navigation system performance. Section V details relevant implementation issues. Results for bias estimation and trimming trajectory performance are presented in Section VI. Finally, Section VII provides concluding remarks on the subject and comments on future work.

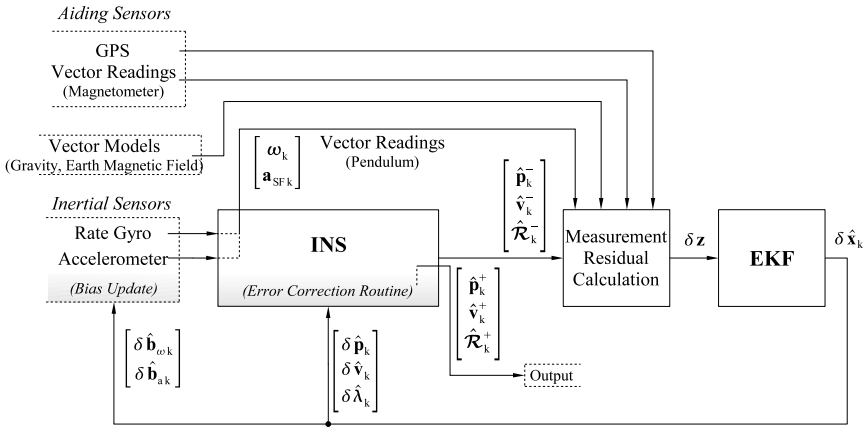

Figure 1. Navigation System Block Diagram

II. Inertial Navigation System Algorithm

In this section, an INS algorithm is briefly introduced, based on the tutorial work that can be found in Ref. 8 for attitude and in Ref. 9 for velocity and position. Angular, velocity and position high-frequency motions, referred to as coning, sculling, and scrolling respectively, are properly accounted for using a multi-rate approach. In this framework, a high-speed, low order algorithm computes dynamic angular rate/acceleration effects at a small sampling interval, and its output is periodically fed to a moderate-speed algorithm that computes attitude/velocity resorting to exact, closed-form equations. Limited operational time and confined mission scenarios for the application at hand allowed to simplify the frame set to Earth and body frames and to adopt an invariant gravity model without loss of precision, while equations were derived to the highest accuracy. Interestingly enough, repetition rate's upper bounds are found to run swift in a standard low-power consumption DSP based hardware architecture. This allows to use maximal precision so that computational accuracy of the INS output is only diminished by the inertial sensors' noise and biases effects.

As depicted in Figure 2, the inputs provided to the inertial algorithms are the integrated inertial sensor

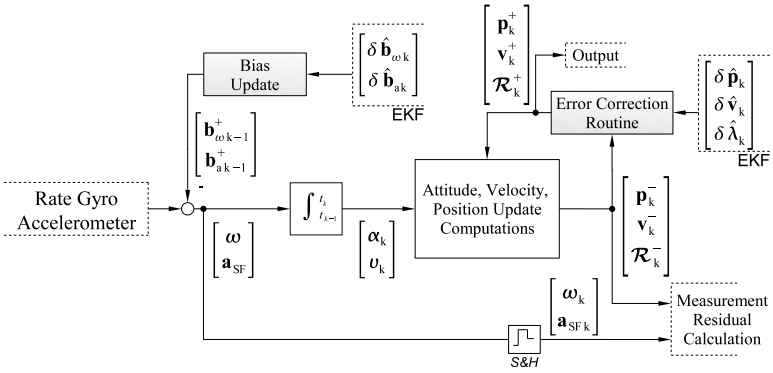

Figure 2. INS with Error and Bias Correction

output increments

$$\boldsymbol{\upsilon}(\tau) = \int_{t_{k-1}}^{\tau} {}^{B}\mathbf{a}_{SF} dt \tag{1}$$

$$\boldsymbol{\alpha}(\tau) = \int_{t_{k-1}}^{\tau} \boldsymbol{\omega} dt \tag{2}$$

where the inertial sensor readings are considered to be corrupted by white noise and bias

$${}^{B}\mathbf{a}_{SF} = {}^{B}\,\bar{\mathbf{a}} + {}^{B}\,\bar{\mathbf{g}} + \bar{\mathbf{b}}_a + \mathbf{n}_a - \mathbf{b}_a \tag{3}$$

$$\boldsymbol{\omega} = \bar{\boldsymbol{\omega}} + \bar{\mathbf{b}}_\omega + \mathbf{n}_\omega - \mathbf{b}_\omega \tag{4}$$

Attitude moderate-speed algorithm[8] computes body attitude in DCM form

$${}^{B_{k-1}}_{B_k}\mathbf{R}(\boldsymbol{\lambda}_k) = \mathbf{I}_{3\times 3} + \frac{\sin\lambda_k}{\lambda_k}\left[\boldsymbol{\lambda}_k\times\right] + \frac{1-\cos\lambda_k}{\lambda_k^2}\left[\boldsymbol{\lambda}_k\times\right]^2 \tag{5}$$

where $\{B_k\}$ is the body frame at time k. Rotation vector dynamics, based on Bortz equation,[17] are formulated in order to denote angular integration and coning attitude terms $\boldsymbol{\alpha}_k$ and $\boldsymbol{\beta}_k$, respectively

$$\boldsymbol{\lambda}_k = \boldsymbol{\alpha}_k + \boldsymbol{\beta}_k \tag{6}$$

where $\boldsymbol{\alpha}_k = \boldsymbol{\alpha}(t)|_{t=t_k}$ and the coning attitude term measures the attitude changes due to the effects of angular rate vector rotation. A high-speed attitude algorithm is required to compute $\boldsymbol{\beta}_k$ as a summation of the high-frequency angular rate vector changes using simple, recursive computations.[8] Equations (5) and (6) summarize both the moderate and high-speed attitude dynamics in the DCM format using exact, error-free equations, enabling high-accuracy results.

Exact linear velocity updates can be computed at moderate-speed rate using the equivalence between strapdown attitude and velocity/position algorithms,[11] that yields

$$\mathbf{v}_k = \mathbf{v}_{k-1} + {}^{E}_{B_{k-1}}\mathbf{R}\Delta^{B_{k-1}}\mathbf{v}_{SF\ k} + \Delta\mathbf{v}_{G/Cor\ k} \tag{7}$$

where $\Delta^{B_{k-1}}\mathbf{v}_{SF\ k}$ is the velocity increment related to the specific force, and $\Delta\mathbf{v}_{G/Cor\ k}$ represents the velocity increment due to gravity and Coriolis effects, see Ref. 9 for further details. High-speed velocity rotation and high-frequency dynamic variations due to angular rate vector rotation, are likewise accounted for in the high-frequency algorithm and included in the moderate-speed calculations as[9]

$$\Delta^{B_{k-1}}\mathbf{v}_{SF\ k} = \boldsymbol{\upsilon}_k + \Delta\mathbf{v}_{rot\ k} + \Delta\mathbf{v}_{scul\ k} \tag{8}$$

where $\boldsymbol{\upsilon}_k = \boldsymbol{\upsilon}(t)|_{t=t_k}$ and $\Delta\mathbf{v}_{rot\ k}$ and $\Delta\mathbf{v}_{scul\ k}$ represent velocity increments due to rotation and sculling, respectively.

III. Extended Kalman Filter Algorithm

In a stand alone INS, bias and inertial sensor errors compensation is usually performed offline. The usage of filtering techniques in navigation systems allows to dynamically compute the biases estimates and to effectively bound the INS errors. The EKF state space model, used in this work, is derived based on the attitude vector dynamics. The sensor's noise characteristics are directly included in the covariance matrices and attitude error compensation does not require attitude normalization procedures. Linearization assumption is kept valid by executing error correction routines and resetting error estimates after each EKF cycle.

A. Error State Space Model

The EKF error equations, based on perturbational rigid body kinematics, were brought to full detail by Britting,[18] and were applied to local navigation in Ref. 14. The attitude, velocity, and position error dynamics can be written as

$$\begin{cases} \delta\dot{\mathbf{p}} = \delta\mathbf{v} \\ \delta\dot{\mathbf{v}} = \mathcal{R}\delta^{B}\mathbf{a}_{SF} - [\mathcal{R}^{B}\mathbf{a}_{SF}\times]\delta\boldsymbol{\lambda} \\ \delta\dot{\boldsymbol{\lambda}} = \mathcal{R}\delta\boldsymbol{\omega} \end{cases} \tag{9}$$

where ${}^{B}\mathbf{a}_{SF} = {}^{B}\mathbf{a} + {}^{B}\mathbf{g}$. Using the rotation error matrix definition[18] $\mathcal{R}(\delta\boldsymbol{\lambda}) \triangleq \mathcal{R}\bar{\mathcal{R}}'$, the attitude error rotation vector $\delta\boldsymbol{\lambda}$, expressed in $\{E\}$, is given by the first order approximation of DCM form (5)

$$\mathcal{R}(\delta\boldsymbol{\lambda}) \simeq \mathbf{I}_{3\times3} + [\delta\boldsymbol{\lambda}\times] \Rightarrow [\delta\boldsymbol{\lambda}\times] \simeq \mathcal{R}\bar{\mathcal{R}}' - \mathbf{I}_{3\times3} \tag{10}$$

Error dynamics (9) are extended to include bias estimation errors using equations (3) and (4) to rewrite the accelerometer and rate gyro additive errors as

$$\begin{aligned} \delta^{B}\mathbf{a}_{SF} &= -\delta\mathbf{b}_{a} + \mathbf{n}_{a} \\ \delta\boldsymbol{\omega} &= -\delta\mathbf{b}_{\omega} + \mathbf{n}_{\omega} \end{aligned} \tag{11}$$

Replacing in (9), the complete error state space model is

$$\begin{cases} \delta\dot{\mathbf{p}} = \delta\mathbf{v} \\ \delta\dot{\mathbf{v}} = -\mathcal{R}\delta\mathbf{b}_{a} - [\mathcal{R}^{B}\mathbf{a}_{SF}\times]\delta\boldsymbol{\lambda} + \mathcal{R}\mathbf{n}_{a} \\ \delta\dot{\boldsymbol{\lambda}} = -\mathcal{R}\delta\mathbf{b}_{\omega} + \mathcal{R}\mathbf{n}_{\omega} \\ \delta\dot{\mathbf{b}}_{a} = -\mathbf{n}_{b_a} \\ \delta\dot{\mathbf{b}}_{\omega} = -\mathbf{n}_{b_\omega} \end{cases} \tag{12}$$

where $\mathbf{n}_{b_a}$, $\mathbf{n}_{b_\omega}$ are zero mean white noises, and the inertial sensors biases are modeled as random walk processes, $\dot{\mathbf{b}}_{a} = \mathbf{n}_{b_a}, \dot{\mathbf{b}}_{\omega} = \mathbf{n}_{b_\omega}$.

The continuous-time error state space model $\delta\dot{\mathbf{x}} = \mathbf{F}(\mathbf{x})\delta\mathbf{x} + \mathbf{G}(\mathbf{x})\mathbf{n}_{x}$ is described by

$$\begin{cases} \delta\hat{\mathbf{x}} = \begin{bmatrix} \delta\hat{\mathbf{p}}' & \delta\hat{\mathbf{v}}' & \delta\hat{\boldsymbol{\lambda}}' & \delta\hat{\mathbf{b}}_{a}' & \delta\hat{\mathbf{b}}_{\omega}' \end{bmatrix}' \\ \mathbf{n}_{x} = \begin{bmatrix} \mathbf{n}_{p}' & \mathbf{n}_{a}' & \mathbf{n}_{\omega}' & \mathbf{n}_{b_a}' & \mathbf{n}_{b_\omega}' \end{bmatrix}' \end{cases}$$

$$\begin{aligned} \mathbf{F}(\mathbf{x}) &= \begin{bmatrix} \mathbf{0} & \mathbf{I} & \mathbf{0} & \mathbf{0} & \mathbf{0} \\ \mathbf{0} & \mathbf{0} & -[\mathcal{R}^{B}\mathbf{a}_{SF}\times] & -\mathcal{R} & \mathbf{0} \\ \mathbf{0} & \mathbf{0} & \mathbf{0} & \mathbf{0} & -\mathcal{R} \\ \mathbf{0} & \mathbf{0} & \mathbf{0} & \mathbf{0} & \mathbf{0} \\ \mathbf{0} & \mathbf{0} & \mathbf{0} & \mathbf{0} & \mathbf{0} \end{bmatrix} \\ \mathbf{G}(\mathbf{x}) &= \texttt{blkdiag}(\mathbf{I}_{3\times3}, \mathcal{R}, \mathcal{R}, -\mathbf{I}_{3\times3}, -\mathbf{I}_{3\times3}) \end{aligned} \tag{13}$$

where `blkdiag`(...) represents a block diagonal matrix and $\mathbf{n}_{p}$ is a fictitious zero mean white noise associated to the position error estimate.

B. Error Compensation

After each EKF update, error estimates are fed into the INS error correction routines as depicted in Figures 1 and 2. It is important to stress that linearization assumptions are kept valid during the algorithm execution since the EKF error estimates are reset after being used to compensate the corresponding variables. The error correction procedures are specific to the INS algorithms and error state space representations. For the INS described in Section II, error routines are detailed next.

Attitude estimate, $\mathcal{R}_k^-$, is compensated using the rotation error matrix $\mathcal{R}(\delta\boldsymbol{\lambda})$ definition, which yields

$$\mathcal{R}_k^+ = \mathcal{R}'_k(\delta\hat{\boldsymbol{\lambda}}_k)\mathcal{R}_k^- \tag{14}$$

where matrix $\mathcal{R}'_k(\delta\hat{\boldsymbol{\lambda}}_k)$ is described exactly as

$$\mathcal{R}'_k(\delta\hat{\boldsymbol{\lambda}}_k) = \mathbf{I}_{3\times3} - \frac{\sin(\left\|\delta\hat{\boldsymbol{\lambda}}_k\right\|)}{\left\|\delta\hat{\boldsymbol{\lambda}}_k\right\|}\left[\delta\hat{\boldsymbol{\lambda}}_k\times\right] + \frac{1-\cos(\left\|\delta\hat{\boldsymbol{\lambda}}_k\right\|)}{\left\|\delta\hat{\boldsymbol{\lambda}}_k\right\|^2}\left[\delta\hat{\boldsymbol{\lambda}}_k\times\right]^2 \tag{15}$$

and is computationally implemented using power series expansion of the scalar trigonometric terms up to an arbitrary accuracy.[12] In the case where few computational resources are available, $\mathcal{R}'_k(\delta\hat{\boldsymbol{\lambda}}_k)$ can be approximated to first order by $\mathcal{R}'_k(\delta\hat{\boldsymbol{\lambda}}_k) \simeq \mathbf{I}_{3\times3} - \left[\delta\hat{\boldsymbol{\lambda}}_k\times\right]$ that, nonetheless, introduces DCM orthogonalization problems in $\mathcal{R}_k^+$ whose compensation usually requires considerable computational effort.[19] The remaining state variables are simply compensated using

$$\begin{aligned}
\mathbf{p}_k^+ &= \mathbf{p}_k^- - \delta\hat{\mathbf{p}}_k \\
\mathbf{v}_k^+ &= \mathbf{v}_k^- - \delta\hat{\mathbf{v}}_k \\
\mathbf{b}_{a\,k}^{\ +} &= \mathbf{b}_{a\,k}^{\ -} - \delta\hat{\mathbf{b}}_{a\,k} \\
\mathbf{b}_{\omega\,k}^{\ +} &= \mathbf{b}_{\omega\,k}^{\ -} - \delta\hat{\mathbf{b}}_{\omega\,k}
\end{aligned} \tag{16}$$

The INS block structure with EKF corrections is depicted in Figure 2, where the error compensation and bias update routines, (14) and (16), are executed after the INS outputs have been fed to the EKF and errors estimates are available. Note that the EKF sampling rate is synchronized with the moderate-speed INS output rate and that no corrections are involved in the high-speed computation algorithms. After the error correction procedure is completed, the EKF error estimates are reset $\delta\hat{\mathbf{x}}_k$=0. At the start of the next computation cycle ($t = t_{k+1}$), the INS attitude and velocity/position updates from Section II are performed on the corrected estimates ($\mathcal{R}_k^+, \mathbf{v}_k^+, \mathbf{p}_k^+$) to provide new inputs ($\mathcal{R}_{k+1}^-, \mathbf{v}_{k+1}^-, \mathbf{p}_{k+1}^-$) to the EKF.

IV. Vector Aiding Techniques

The EKF relies on aiding sensor readings to successfully estimate the error states. The physical coupling between attitude and velocity errors (9) enables the use of GPS position readings to partially estimate attitude errors. As convincingly argued by Goshen-Meskin,[3] for observability analysis purposes a GPS based navigation system with bias estimation can be split into a concatenation of piece-wise time-invariant systems with little loss of accuracy and, under that assumption, full observability is met by performing specific maneuvers along the flight path. Even though the GPS itself does not suffice to implement a fully observable navigation system, in-flight characteristic maneuvers and disturbances are shown to alternately excite the non-observable variables. This circle of ideas directed the scientific community research effort towards including additional aiding sources to strengthen the system observability for typical vehicle maneuvers, see Refs. 4–6.

The vector observation technique major contribution is to enhance the system observability by providing attitude observations and vehicle dynamics bandwidth information to the EKF. Reference 1 previously derived a self-contained device to compute attitude matrix $\mathcal{R}_{MPS}$ using the magnetometer triad readings and the Earth's gravitational field available from processing the accelerometer triad measurements. The attitude measurement residual $\delta\mathbf{z}_{\lambda\ MPS}$ presented to the filter was described by

$$[\delta\mathbf{z}_{\lambda\ MPS}\times] = \mathcal{R}\mathcal{R}'_{MPS} - \mathbf{I}_{3\times3} \tag{17}$$

and modeled in the filter as

$$\delta \mathbf{z}_{\lambda\ MPS} = \delta\boldsymbol{\lambda} + \mathbf{n}_{MPS} \tag{18}$$

using a noise term $\mathbf{n}_{MPS}$ to compensate for the magnetometer, accelerometer, rate gyro and INS disturbances impact on the attitude algorithm. Nonetheless, characterizing $\mathbf{n}_{MPS}$ as white noise could degrade the filter performance because it did not properly model the non-linear influence of inertial/magnetic sensors errors in $\mathcal{R}_{MPS}$ computations.

In this work, vector observations are directly embedded in the EKF, as depicted in Figure 1. The gravity selective frequency contents provided by the accelerometer triad yield a precise $\mathbf{n}_{MPS}$ equivalent, endowing the filter with a much more clear and accurate stochastic description of the navigation system error sources and disturbances.

The EKF implicitly computes the attitude based on the vector observations, presenting an alternate optimal solution to the Wahba's problem[20] that encloses system dynamics, without external attitude determination algorithms and using actual optimal criteria. Sensor error characteristics other than just white noise are properly modeled in the filter, using the EKF covariance matrices and the structure of the error state space model. The algorithm presented herein can be generalized to any number of vector observations, devising a straightforward procedure to enhance the accuracy of the navigation system results which also reinforces the EKF linearization assumption.

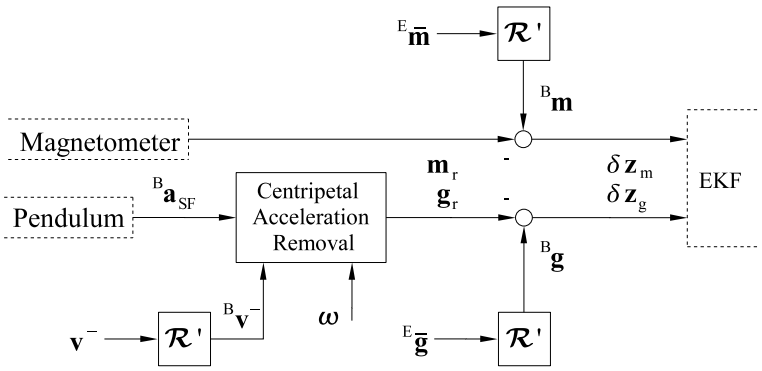

Figure 3. Vector Measurement Residual Computation (Magnetometer and Gravity)

A. General Vector Measurements

Consider a generic vector $\mathbf{s}$, the attitude measurement residual $\delta\mathbf{z}_s = ({}^B\mathbf{s} - \mathbf{s}_r)$ is computed by comparing the vector body frame coordinates readings

$$\mathbf{s}_r = \bar{\mathcal{R}}'^E\bar{\mathbf{s}} + \mathbf{n}_s \tag{19}$$

with the INS estimate

$${}^B\mathbf{s} = \mathcal{R}'^E\bar{\mathbf{s}} \tag{20}$$

Replacing the INS attitude estimate $\mathcal{R}'$ by the attitude error $\delta\boldsymbol{\lambda}$ approximation (10) yields

$$\begin{aligned}\mathbf{s}_r &= \bar{\mathcal{R}}'^E\bar{\mathbf{s}} + \mathbf{n}_s = \mathcal{R}'\left[\mathbf{I}_{3\times3} + \delta\boldsymbol{\lambda}\times\right]^E\bar{\mathbf{s}} + \mathbf{n}_s \\ &=^B \mathbf{s} - \mathcal{R}'\left[{}^E\bar{\mathbf{s}}\times\right]\delta\boldsymbol{\lambda} + \mathbf{n}_s\end{aligned} \tag{21}$$

which relates the EKF measurement residual $\delta\mathbf{z}_r$ with the attitude error $\delta\boldsymbol{\lambda}$, bearing

$$\delta\mathbf{z}_s = \mathcal{R}'\left[{}^E\bar{\mathbf{s}}\times\right]\delta\boldsymbol{\lambda} - \mathbf{n}_s \tag{22}$$

where $\mathbf{n}_s$ is the vector readings sensor noise. An equivalent result for the attitude error expressed in body frame is discussed in the Appendix. In general, other additive sensor disturbances are found in the vector

readings (19). These include sensor errors such as biases $\mathbf{b}_s$ that are compensated in the INS block, or sensor disturbances $\mathbf{d}_s$ whose dynamics are modeled in the EKF filter, bearing

$$\mathbf{s}_r = \bar{\mathcal{R}}'^{E}\bar{\mathbf{s}} + \mathbf{n}_s + \delta\mathbf{b}_s + \mathbf{d}_s \tag{23}$$

where $\delta\mathbf{b}_s$ represents the error term associated to $\mathbf{b}_s$ and $\mathbf{d}_s$ is described by augmenting the EKF state model. The measurement residual is thus described by

$$\delta\mathbf{z}_s = \mathcal{R}'\left[{}^{E}\bar{\mathbf{s}}\times\right]\delta\boldsymbol{\lambda} - \delta\mathbf{b}_s - \mathbf{d}_s - \mathbf{n}_s \tag{24}$$

This result shows how to introduce the aiding sensor measurement residual $\delta\mathbf{z}_s$ in the EKF based on a vector measurement $\mathbf{s}_r$. The derived result applies to the magnetometer readings by replacing the generic vector $\mathbf{s}$ with Earth's magnetic field $\mathbf{m}$, as depicted in Figure 3. The proposed technique enhances the state observability and is suited for an arbitrary number of vector observations. Aiding sensor parameters like noise variances σ_s^2 directly fit in the EKF observation noise covariance matrix, which allows to integrate new attitude sensors without time-consuming parameter tuning procedures.

Intermediate attitude estimates computation is plainly skipped since the vector readings sources are directly modeled and fed into the filter. In review, while the INS calculates the body attitude estimates using high-precision algorithms described in Section II, the EKF main function is to turn aiding sensor readings into attitude, velocity, position error and biases estimates to be fed back into the INS.

B. Frequency Components of Vector Observations

Based on the main result of previous section (24), gravity vector readings are derived from the accelerometer measurements. The gravity vector expressed in the body coordinate system is obtained from the accelerometer triad as

$$\mathbf{g}_r \triangleq^{B} \mathbf{a}_{SF} - \boldsymbol{\omega} \times^{B} \mathbf{v} \tag{25}$$

and is compared to the INS gravity estimate

$${}^{B}\mathbf{g} = \mathcal{R}'^{E}\bar{\mathbf{g}} \tag{26}$$

The INS gravity estimate ${}^{B}\mathbf{g}$ description is identical to the ${}^{B}\mathbf{s}$ definition (20). The accelerometer triad gravity measurement $\mathbf{g}_r$ contains additional acceleration compensation terms (3), yielding

$$\mathbf{g}_r =^{B} \bar{\mathbf{g}} + \mathbf{a}_{LA} - \delta\mathbf{b}_a - \delta\left(\boldsymbol{\omega} \times^{B} \mathbf{v}\right) + \mathbf{n}_a \tag{27}$$

where the $\delta\left(\boldsymbol{\omega} \times^{B} \mathbf{v}\right) = \boldsymbol{\omega} \times^{B} \mathbf{v} - \bar{\boldsymbol{\omega}} \times^{B} \bar{\mathbf{v}}$ is the error related to the centripetal acceleration removal in (25), and $\mathbf{a}_{LA} = \begin{bmatrix} a_{LAx} & a_{LAy} & a_{LAz} \end{bmatrix}'$ represents the linear acceleration. Note that equation (27) is according to the methodology introduced in (23).

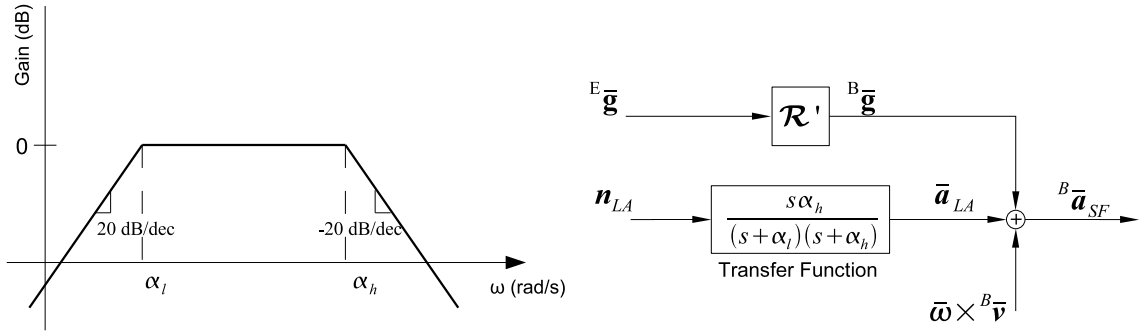

(a) Bode Plot (b) Specific Force Model

Figure 4. Linear Acceleration Characteristics

In general Autonomous Vehicles can only produce linear acceleration for short time periods and their accelerations can be assumed as relatively high frequency signals. Based on this assumption, each of the

$\mathbf{a}_{LA}$ components can be modeled as a band pass signal whose bandwidth is shaped according to the vehicle characteristics, often to filter out high-frequency INS acceleration jitter and to simultaneously avoid the influence of erroneous low-frequency accelerometer bias. The state model dynamics for the x-axis component, is generically represented in Figure 4, and can be written as

$$\dot{\mathbf{x}}_{LA} \triangleq \begin{bmatrix} \dot{x}_{1\ LAx} \\ \dot{x}_{2\ LAx} \end{bmatrix} = \begin{bmatrix} 0 & 1 \\ -\alpha_h\alpha_l & -(\alpha_h+\alpha_l) \end{bmatrix} \begin{bmatrix} x_{1\ LAx} \\ x_{2\ LAx} \end{bmatrix} + \begin{bmatrix} 0 \\ \alpha_h \end{bmatrix} n_{LAx} \tag{28}$$
$$a_{LAx} = x_{2\ LAx}$$

where α_h and α_l are the high-frequency and low-frequency cutoff frequencies, respectively, and n_{LAx} is a white noise input with variance σ^2_{LA}.

The centripetal acceleration compensation term is derived using (4) and (10) to yield

$$\delta\left(\boldsymbol{\omega} \times^B \mathbf{v}\right) = [\boldsymbol{\omega}\times]\,\mathcal{R}'\delta\mathbf{v} + [\boldsymbol{\omega}\times]\left[{}^B\mathbf{v}\times\right]\mathcal{R}'\delta\boldsymbol{\lambda} + \left[{}^B\mathbf{v}\times\right](\delta\mathbf{b}_\omega - \mathbf{n}_\omega) \tag{29}$$

where the first two right-hand-side terms arise from the velocity estimation errors and the third is originated by rate gyro errors.

The gravity measurement residual $\delta\mathbf{z}_g$ is defined by $\delta\mathbf{z}_g = \left({}^B\mathbf{g} - \mathbf{g}_r\right)$, as depicted in Figure 3. Using the previously derived result (24), the vector measurement residual can be expressed as

$$\delta\mathbf{z}_g = \mathcal{R}'\left[{}^E\bar{\mathbf{g}}\times\right]\delta\boldsymbol{\lambda} + \delta\mathbf{b}_a + \delta\left(\boldsymbol{\omega} \times^B \mathbf{v}\right) - \mathbf{a}_{LA} - \mathbf{n}_a \tag{30}$$

Replacing the centripetal acceleration term (29), the complete gravity measurement residual equation yields

$$\delta\mathbf{z}_g = [\boldsymbol{\omega}\times]\,\mathcal{R}'\delta\mathbf{v} + \left(\mathcal{R}'\left[{}^E\bar{\mathbf{g}}\times\right] + [\boldsymbol{\omega}\times]\left[{}^B\mathbf{v}\times\right]\mathcal{R}'\right)\delta\boldsymbol{\lambda} + \delta\mathbf{b}_a + \left[{}^B\mathbf{v}\times\right]\delta\mathbf{b}_\omega - \mathbf{n}_a - \left[{}^B\mathbf{v}\times\right]\mathbf{n}_\omega - \mathbf{a}_{LA} \tag{31}$$

which includes the EKF state augmentation introduced in (28) for vehicle acceleration modeling.

V. Implementation

The complete continuous state model vectors and matrices are

$$\begin{cases} \hat{\mathbf{x}}_C = \begin{bmatrix} \delta\hat{\mathbf{x}}' & \mathbf{x}'_{LAx} & \mathbf{x}'_{LAy} & \mathbf{x}'_{LAz} \end{bmatrix}' \\ \mathbf{n}_{xC} = \begin{bmatrix} \mathbf{n}'_x & n_{LAx} & n_{LAy} & n_{LAz} \end{bmatrix}' \end{cases} \tag{32}$$

$$\mathbf{F}_C(\mathbf{x}) = \texttt{blkdiag}(\mathbf{F}(\mathbf{x}), \mathbf{F}_{LA}, \mathbf{F}_{LA}, \mathbf{F}_{LA}) \tag{33}$$

$$\mathbf{G}_C(\mathbf{x}) = \texttt{blkdiag}(\mathbf{G}(\mathbf{x}), \mathbf{G}_{LA}, \mathbf{G}_{LA}, \mathbf{G}_{LA}) \tag{34}$$

$$\mathbf{F}_{LA} = \begin{bmatrix} 0 & 1 \\ -\alpha_l\alpha_h & -(\alpha_l+\alpha_h) \end{bmatrix}, \mathbf{G}_{LA} = \begin{bmatrix} 0 \\ \alpha_h \end{bmatrix} \tag{35}$$

and the measurements are described using the classical state model observations $\delta\mathbf{z} = \mathbf{H}(\mathbf{x})\,\delta\mathbf{x} + \mathbf{n}_z$ where

$$\begin{cases} \delta\mathbf{z} = \begin{bmatrix} \delta\mathbf{z}'_p & \delta\mathbf{z}'_m & \delta\mathbf{z}'_g \end{bmatrix}' \\ \mathbf{n}_z = \begin{bmatrix} -\mathbf{n}'_{GPS} & -\mathbf{n}'_m & \left(-\mathbf{n}_a - {}^B\mathbf{v}\times\mathbf{n}_\omega + \mathbf{n}_{\delta g}\right)' \end{bmatrix}' \end{cases} \tag{36}$$

$$\mathbf{H}(\mathbf{x}) = \begin{bmatrix} \mathbf{I} & \mathbf{0} & \mathbf{0} & \mathbf{0} & \mathbf{0} & \mathbf{0} \\ \mathbf{0} & \mathbf{0} & \mathcal{R}'\left[{}^E\bar{\mathbf{m}}\times\right] & \mathbf{0} & \mathbf{0} & \mathbf{0} \\ \mathbf{0} & [\boldsymbol{\omega}\times]\,\mathcal{R}' & \mathcal{R}'\left[{}^E\bar{\mathbf{g}}\times\right] + [\boldsymbol{\omega}\times]\left[{}^B\mathbf{v}\times\right]\mathcal{R}' & \mathbf{I}_{3\times3} & \left[{}^B\mathbf{v}\times\right] & \mathbf{H}_{LA} \end{bmatrix} \tag{37}$$

$$\mathbf{H}_{LA} = \texttt{blkdiag}(\begin{bmatrix} 0 & -1 \end{bmatrix}, \begin{bmatrix} 0 & -1 \end{bmatrix}, \begin{bmatrix} 0 & -1 \end{bmatrix}) \tag{38}$$

and $\mathbf{n}_{\delta g}$ is a fictitious white noise associated with $\delta\mathbf{z}_g$ observation. The position measurement residual $\delta\mathbf{z}_p$ is classically obtained from the GPS readings.[14]

The state and observation noise covariance matrices are

$$\mathbf{Q}_C = \texttt{blkdiag}(\sigma^2_p\mathbf{I}_{3\times3}, \sigma^2_v\mathbf{I}_{3\times3}, \sigma^2_\omega\mathbf{I}_{3\times3}, \sigma^2_{b_a}\mathbf{I}_{3\times3}, \sigma^2_{b_\omega}\mathbf{I}_{3\times3}, \sigma^2_{LA}\mathbf{I}_{3\times3}) \tag{39}$$

$$\mathbf{R}_C(\mathbf{x}) = \texttt{blkdiag}(\sigma^2_{GPS}\mathbf{I}_{3\times3}, \sigma^2_m\mathbf{I}_{3\times3}, \sigma^2_a\mathbf{I}_{3\times3} - \sigma^2_\omega[{}^B\mathbf{v}\times]^2) \tag{40}$$

The discrete-time state space model is obtained using the zero order hold discretization technique

$$\mathbf{\Phi}_k = e^{F_k T}, \mathbf{H}_k = \mathbf{H}(\mathbf{x})|_{t=t_k} \tag{41}$$

and the discrete-time noise covariance matrices are[21]

$$\mathbf{Q}_k \simeq [\mathbf{G}_k \mathbf{Q}_C \mathbf{G}_k']T, \mathbf{R}_k \simeq \frac{\mathbf{R}_{Ck}}{T} \tag{42}$$

where T is the sampling period, $\mathbf{F}_k = \mathbf{F}_C(\mathbf{x})|_{t=t_k}$, $\mathbf{G}_k = \mathbf{G}_C(\mathbf{x})|_{t=t_k}$, $\mathbf{R}_{Ck} = \mathbf{R}_C(\mathbf{x})|_{t=t_k}$ and $\mathbf{\Phi}_k = \mathbf{\Phi}(t_{k+1}, t_k)$ denotes the state transition matrix.

The gravity measurement residual $\delta\mathbf{z}_g$ introduces state and measurement noise correlation matrix[22]

$$\mathbf{C}_C(\mathbf{x}) = \begin{bmatrix} \mathbf{0} & \mathbf{0} & \mathbf{0} & \mathbf{0} & \mathbf{0} & \mathbf{0} \\ \mathbf{0} & \mathbf{0} & \mathbf{0} & \mathbf{0} & \mathbf{0} & \mathbf{0} \\ \mathbf{0} & -\sigma_a^2 \mathbf{I}_{3\times 3} & \sigma_\omega^2 [{}^B\mathbf{v}\times]' & \mathbf{0} & \mathbf{0} & \mathbf{0} \end{bmatrix}' \tag{43}$$

$$\mathbf{C}_k = \frac{1}{T}\int_{t_{k-1}}^{t_k} \boldsymbol{\phi}(t_k, \tau)\, \mathbf{G}(\tau)\, \mathbf{C}_C(\tau)\, d\tau \simeq (\mathbf{I}_{3\times 3} + \frac{\mathbf{F}_k T}{2})\mathbf{G}_k \mathbf{C}_{Ck} \tag{44}$$

where $\mathbf{C}_C(\mathbf{x})$ is the continuous state and measurement noises correlation matrix and $\mathbf{C}_{Ck} = \mathbf{C}_C(\mathbf{x})|_{t=t_k}$. The discrete-time equivalent matrix $\mathbf{C}_k$ is computed using a first order approximation similar to those discussed in Ref. 22 for $\mathbf{Q}_k$ and $\mathbf{R}_k$. The following Kalman gains and error covariance matrix equations are adapted to include the state and measurement noises correlation matrix

$$\mathbf{K}_k = (\mathbf{P}_k^- \mathbf{H}_k' + \mathbf{C}_k)[\mathbf{H}_k \mathbf{P}_k^- \mathbf{H}_k' + \mathbf{R}_k + \mathbf{H}_k \mathbf{C}_k + \mathbf{C}_k' \mathbf{H}_k']^{-1} \tag{45}$$

$$\mathbf{P}_k^+ = (\mathbf{I}_{n\times n} - \mathbf{K}_k \mathbf{H}_k)\mathbf{P}_k^- - \mathbf{K}_k \mathbf{C}_k' \tag{46}$$

and the filter covariance matrix is updated using $\mathbf{P}_{k+1}^- = \mathbf{\Phi}_k \mathbf{P}_k^+ \mathbf{\Phi}_k' + \mathbf{Q}_k$.

VI. Results

The impact of the magnetometer and gravity vector measurements on the system performance is assessed next using three case study simulations. The first simulation sets initial alignment errors in order to evidence the gravity vector measurement role on tackling the filter estimation errors. The second simulation focuses on the filter's ability to estimate linear acceleration by processing the selective frequency contents from the accelerometer readings. The third simulation assesses the navigation system performance about a standard trimming trajectory, with constant centripetal acceleration. In addition, the event of sparse/unavailable GPS signal is studied to point out how the position estimates are smoothed by the gravity vector measurements.

The INS high-speed algorithm is set to run at 100 Hz and the normal-speed algorithm is synchronized with the EKF, both executed at 50Hz. The GPS provides position measurements at the nominal frequency of 1Hz. The noise and bias characteristics of the sensors are presented in Table 1.

Table 1. Sensor Errors

Sensor	**Bias**	**Noise Variance** (σ^2)
Rate Gyro	0.05 °/s	$(0.02\ °/s)^2$
Accelerometer	10 mg	$(0.6\ mg)^2$
Magnetometer	-	$(1\ \mu G)^2$
GPS	-	$10\ m^2$

A. Initial Alignment Error

The contribution of the gravity selective frequency contents on the state variables estimation is shown in simulations for the following initial misalignment cases

a. Roll angle: $\delta\phi = 5^o$;

b. Body frame x-axis rate gyro bias: $\delta b_{\omega x} = 0.57^o/\text{s}$;

c. Body frame z-axis accelerometer: $\delta b_{az} = 1\text{mg}$.

The vehicle is subject to constant linear and centripetal acceleration inputs, thus describing an ascending helix (trimming) trajectory, as depicted in Figure 5(a). Results show that the gravity vector readings improve the GPS and magnetometer combination, as errors converge to zero in less than 10 seconds. As depicted in Figure 5, the rate gyro bias, roll angle ϕ and vertical accelerometer bias $\bar{b}_{az}$ estimation is enhanced by the gravity vector readings. Interestingly enough, position and velocity error build up due to ill gravity compensation are reduced by the proposed compensation technique.

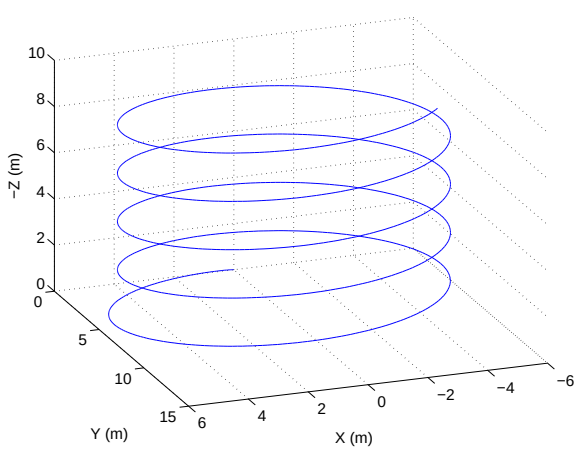

(a) Trimming Trajectory

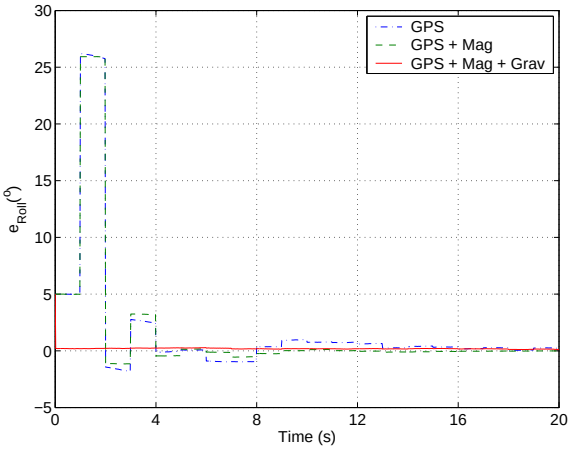

(b) Roll Misalignment

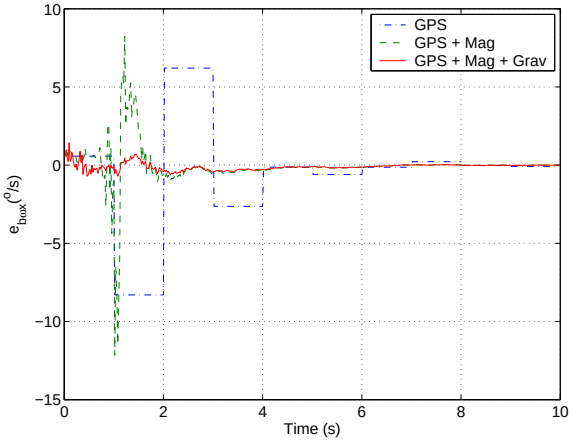

(c) Rate Gyro Bias Misalignment

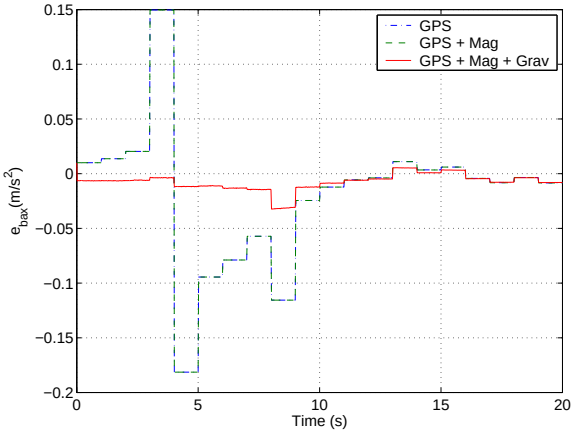

(d) Accelerometer Bias Misalignment

Figure 5. Misalignment Estimation

B. Linear Accelerated Motion

The second simulation is run for a straight line trajectory with initial acceleration along the x-axis, Figure 6(a). In this experiment, vehicle velocity increases until the input acceleration is compensated by the linear drag effects, as depicted in Figure 6(a), and linear uniform motion is attained. Figure 6(b) validates the assumption that autonomous vehicle's linear acceleration can effectively be modeled as a band pass signal (28), leaving the gravity vector low frequency contents free to successfully improve INS errors. Numerical results obtained with the proposed technique are presented in Table 2, where improvements due to the inclusion of aiding vector observations are evident.

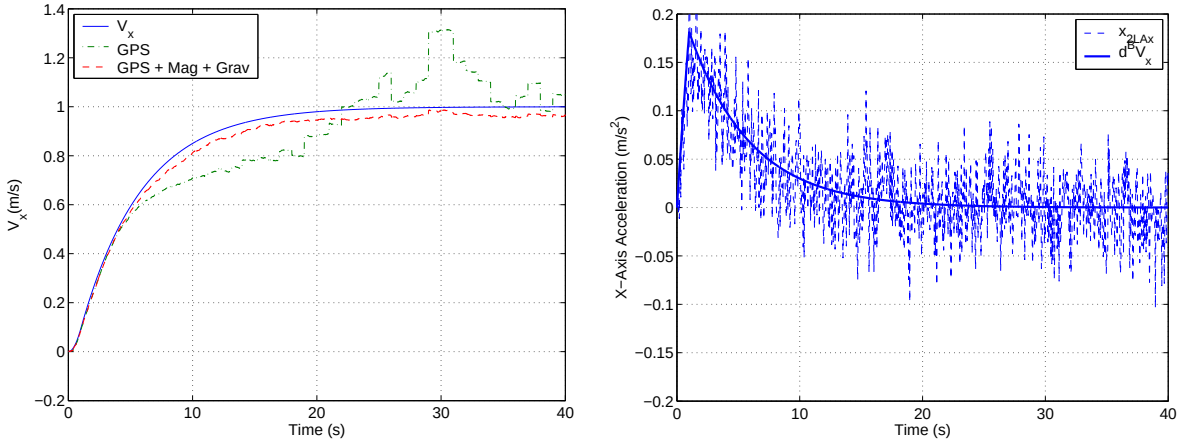

(a) Velocity Profile

(b) Linear Acceleration Estimation

Figure 6. Linear Accelerated Motion Results

Table 2. Filter Results, Straight Path Trajectory

	Average Square Error					
	X	Y	Z	Yaw	Pitch	Roll
$\delta\mathbf{z} = \delta\mathbf{z}_p$	1.08 m	0.39 m	0.16 m	2.90×10^{-4} °	6.90×10^{-5} °	1.79×10^{-4} °
$\delta\mathbf{z} = \begin{bmatrix} \delta\mathbf{z}_p \\ \delta\mathbf{z}_m \\ \delta\mathbf{z}_g \end{bmatrix}$	0.24 m	0.23 m	0.15 m	5.64×10^{-11} °	6.04×10^{-11} °	1.54×10^{-4} °

C. Trimming Trajectory

The long term navigation system behavior is assessed in simulation about an Unmanned Aerial Vehicle standard trimming trajectory without initial alignment errors, although inertial sensor noise and bias are present. Navigation system position estimates are compared in Figure 7 for the single GPS and for the proposed technique. Numerical results are brought to detail in Table 3.

Figure 7 depicts the performance enhancements introduced by the magnetometer readings and the selective frequency contents of the accelerometers measurements. Adding the magnetometer readings clearly smoothes out yaw errors, as presented in Table 3. Due to the position and attitude errors correlation (12), x-axis position errors are also improved. Finally, the gravity readings are found to help attitude and position estimation, despite the constant centripetal acceleration in the trimming trajectory and the initial linear acceleration.

The gravity readings contribution is more noticeable in the case of a sparse GPS signal. Simulations for a GPS signal with output frequency of $\frac{1}{15}$ Hz are depicted in Figure 8. The figure shows that x and y axes position estimates are enhanced by the selective frequency contents of the accelerometers measurements., which extends the navigation system autonomy with respect to the GPS aiding source.

Table 3. Filter Results, Trimming Trajectory

	Average Square Error					
	X	Y	Z	Yaw	Pitch	Roll
$\delta \mathbf{z} = \delta \mathbf{z}_p$	1.22 m	2.21 m	0.88 m	1.58 °	2.37×10^{-4} °	1.79×10^{-4} °
$\delta \mathbf{z} = \begin{bmatrix} \delta \mathbf{z}_p \\ \delta \mathbf{z}_m \end{bmatrix}$	0.44 m	2.27 m	0.86 m	1.46×10^{-10} °	1.37×10^{-4} °	1.20×10^{-4} °
$\delta \mathbf{z} = \begin{bmatrix} \delta \mathbf{z}_p \\ \delta \mathbf{z}_m \\ \delta \mathbf{z}_g \end{bmatrix}$	0.42 m	1.90 m	0.86 m	1.28×10^{-10} °	1.25×10^{-4} °	1.04×10^{-4} °

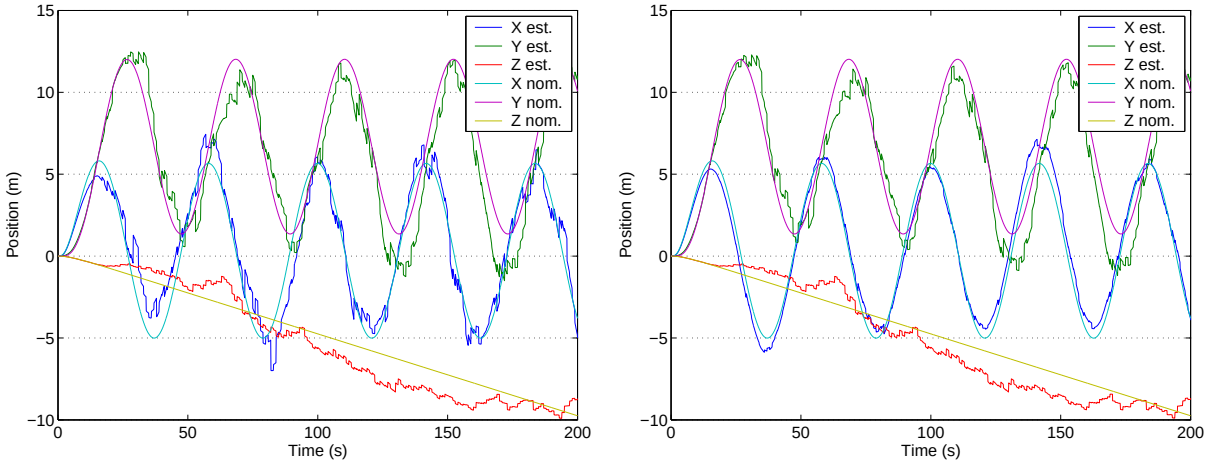

(a) Single GPS

(b) GPS, Magnetic field and Gravity Readings

Figure 7. Trimming Trajectory Results

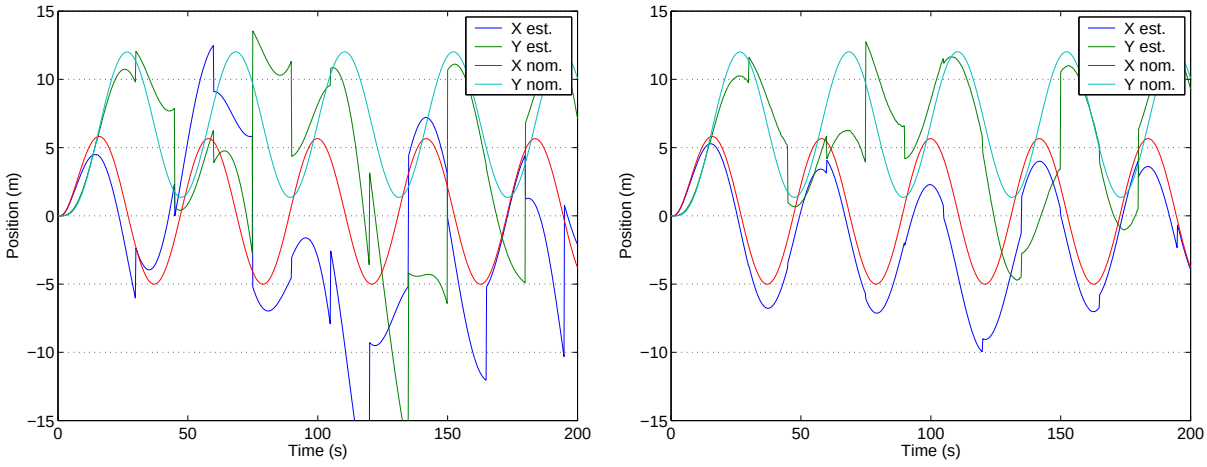

(a) Single GPS

(b) GPS and Gravity Readings

Figure 8. Sparse GPS Signal Results

VII. Conclusion

An aiding technique to enhance strapdown inertial navigation systems error estimation was presented and discussed. An advanced, Global Positioning System/Inertial Navigation System (GPS/INS) using Extended Kalman Filter (EKF) was outlined and an aiding technique that resorts to the use of selective frequency contents from vector readings was detailed. From the performance results obtained with the INS aiding architecture applied to typical UAV trajectories, it became clear that inertial sensors' misalignment errors can be estimated resorting to the gravity vector low frequency information embodied in the accelerometer measurements. Moreover, the navigation system accuracy and autonomy with respect to GPS were improved. Future work will focus on implementation issues of the proposed high-accuracy, multi-rate integrated GPS/INS architecture on a low-power consumption DSP based hardware. Hands-on tests will be run on a Vario X-Treme model-scale helicopter, property of the Institute for Systems and Robotics.

Acknowledgments

This work was partially supported by the FCT Programa Operacional da Sociedade de Informação (POSI) in the frame of QCA III and by the POSI/SRI/41938/2001 ALTICOPTER project. The work of J.F. Vasconcelos was supported by a PhD Student Scholarship, SFRH/BD/18954/2004, from the Portuguese FCT POCTI programme.

Appendix: Attitude Error Coordinate Frame

Interestingly enough, some filters represent the attitude error in body frame coordinates[15,16]

$$^{B}\delta\boldsymbol{\lambda} = \mathcal{R}'\delta\boldsymbol{\lambda} \tag{47}$$

Using Coriolis theorem, which relates general vector $\mathbf{r}$ dynamics in body ($^{B}\mathbf{r}$) and Earth ($^{E}\mathbf{r}$) frames coordinates,

$$\frac{d}{dt}^{B}\mathbf{r} = \mathcal{R}'\frac{d}{dt}^{E}\mathbf{r} - \boldsymbol{\omega} \times^{B} \mathbf{r} \tag{48}$$

and replacing $\mathbf{r}$ by $\delta\boldsymbol{\lambda}$, yields

$$\frac{d}{dt}^{B}\delta\boldsymbol{\lambda} = \mathcal{R}'\frac{d}{dt}\delta\boldsymbol{\lambda} - \boldsymbol{\omega} \times^{B} \delta\boldsymbol{\lambda}. \tag{49}$$

From $\delta\boldsymbol{\lambda}$ rotation vector dynamics (12), the $^{B}\delta\boldsymbol{\lambda}$ dynamics are retrieved

$$\begin{aligned}
&\frac{d}{dt}^{B}\delta\boldsymbol{\lambda} = \mathcal{R}'(-\mathcal{R}\delta\mathbf{b}_{\omega} + \mathcal{R}\mathbf{n}_{\omega}) - \boldsymbol{\omega} \times^{B} \delta\boldsymbol{\lambda} \Rightarrow \\
&\frac{d}{dt}^{B}\delta\boldsymbol{\lambda} = -\boldsymbol{\omega} \times^{B} \delta\boldsymbol{\lambda} - \delta\mathbf{b}_{\omega} + \mathbf{n}_{\omega}
\end{aligned} \tag{50}$$

setting the correspondence between the current EKF dynamics and the results derived in Refs. 15, 16.

If the attitude error is depicted in body coordinate frame, the proper observation equation is obtained using cross-product matrix properties in (22)

$$\delta\mathbf{z}_r = \mathcal{R}'\left[^{E}\bar{\mathbf{r}}\times\right]\delta\boldsymbol{\lambda} - \mathbf{n}_r = \left[\mathcal{R}'\ ^{E}\bar{\mathbf{r}}\times\right]\mathcal{R}'\delta\boldsymbol{\lambda} - \mathbf{n}_r = \left[^{B}\mathbf{r}\times\right]^{B}\delta\boldsymbol{\lambda} - \mathbf{n}_r \tag{51}$$

Due to the equivalency in first order attitude error parameterizations, eqs. (50) and (51) hold for rotation vector, Gibbs vector and Modified Rodrigues Parameters.

References

[1]Vasconcelos, J., Calvário, J., Oliveira, P., and Silvestre, C., "GPS Aided IMU for Unmanned Air Vehicles," *Proceedings of the 5th IFAC/EURON Symposium on Intelligent Autonomous Vehicles (IAV2004)*, IST, Lisbon, Portugal, July 2004.

[2]Goshen-Meskin, D. and Bar-Itzhack, I., "Observability Analysis of Piece-Wise Constant Systems - Part I: Theory," *IEEE Transactions On Aerospace and Electronic Systems*, Vol. 28, No. 4, October 1992, pp. 1056–1067.

[3]Goshen-Meskin, D. and Bar-Itzhack, I., "Observability Analysis of Piece-Wise Constant Systems - Part II: Application to Inertial Navigation In-Flight Alignment," *IEEE Transactions On Aerospace and Electronic Systems*, Vol. 28, No. 4, October 1992, pp. 1068–1075.

[4]Bar-Itzhack, I. and Harman, R., "The Effect of Sensor Failure on the Attitude and Rate Estimation of the MAP Space-Craft," *AIAA Guidance, Navigation and Control Conference*, 2003.

[5]Ma, X., Sukkarieh, S., and Kim, J., "Vehicle Model Aided Inertial Navigation," *Proceedings of the IEEE Intelligent Transportation Systems*, Vol. 2, Shangai, China, 2003, pp. 1004–1009.

[6]Koifman, M. and Bar-Itzhack, I., "Inertial Navigation System Aided by Aircraft Dynamics," *IEEE Transactions on Control Systems Technology*, Vol. 7, No. 4, 1999, pp. 487–493.

[7]Choukroun, D., *Novel Methods for Attitude Determination Using Vector Observations*, Ph.D. thesis, Israel Institute of Technology, May 2003.

[8]Savage, P., "Strapdown Inertial Navigation Integration Algorithm Design Part 1: Attitude Algorithms," *AIAA Journal of Guidance, Control, and Dynamics*, Vol. 21, No. 1, January-February 1998, pp. 19–28.

[9]Savage, P., "Strapdown Inertial Navigation Integration Algorithm Design Part 2: Velocity and Position Algorithms," *AIAA Journal of Guidance, Control, and Dynamics*, Vol. 21, No. 2, March-April 1998, pp. 208–221.

[10]Ignagni, M., "Duality of Optimal Strapdown Sculling and Coning Compensation Algorithms," *Journal of the Institute of Navigation*, Vol. 45, No. 2, Summer 1998, pp. 85–95.

[11]Roscoe, K., "Equivalency Between Strapdown Inertial Navigation Coning and Sculling Integrals/Algorithms," *AIAA Journal of Guidance, Control, and Dynamics*, Vol. 24, No. 2, 2001, pp. 201–205.

[12]Savage, P., *Strapdown Analytics*, Vol. 1, Strapdown Associates, Inc., Maple Plain, MN, 2000.

[13]Gaylor, D., *Integrated GPS/INS Navigation System for Design for Autonomous Spacecraft Rendezvous*, Ph.D. thesis, The Univesity of Texas at Austin, 2003.

[14]Sukkarieh, S., *Low Cost, High Integrity, Aided Inertial Navigation Systems for Autonomous Land Vehicles*, Ph.D. thesis, University of Sydney, 2000.

[15]Markley, F., "Attitude Error Representations for Kalman Filtering," *AIAA Journal of Guidance, Control, and Dynamics*, Vol. 26, No. 2, March-April 2003, pp. 311–317.

[16]Pittelkau, M., "Rotation Vector in Attitude Estimation," *AIAA Journal of Guidance, Control, and Dynamics*, Vol. 26, No. 6, November-December 2003, pp. 855–860.

[17]Bortz, J., "A New Mathematical Formulation for Strapdown Inertial Navigation," *IEEE Transactions on Aerospace and Electronic Systems*, Vol. 7, No. 1, 1971, pp. 61–66.

[18]Britting, K., *Inertial Navigation Systems Analysis*, John Wiley & Sons, Inc., 1971.

[19]Choukroun, D., Weiss, H., Bar-Itzhack, I., and Oshman, Y., "Direction Cosine Matrix Estimation Form Vector Observations Using a Matrix Kalman Filter," *AIAA Guidance, Navigation and Control Conference*, 2003.

[20]Wahba, G., "A Least-Squares Estimate of Satellite Attitude," *SIAM Review*, Vol. 7, No. 3, 1965, pp. 409 problem 65–1.

[21]Gelb, A., *Applied Optimal Estimation*, MIT Press, 1974.

[22]Brown, R. and Hwang, P., *Introduction to Random Signals and Applied Kalman Filtering*, John Wiley & Sons, Inc., 3rd ed., 1997.